Cotunneling enhancement of magnetoresistance in double magnetic tunnel junctions with embedded superparamagnetic NiFe nanoparticles

K. J. Dempsey,[1,*] A. T. Hindmarch,[1] H.-X. Wei,[2] Q.-H. Qin,[2] Z.-C. Wen,[2] W.-X. Wang,[2] G. Vallejo-Fernandez,[3] D. A. Arena,[4] X.-F. Han,[2] and C. H. Marrows[1,†]

[1]*School of Physics and Astronomy, University of Leeds, Leeds LS2 9JT, United Kingdom*

[2]*State Key Laboratory of Magnetism, Beijing National Laboratory for Condensed Matter Physics, Institute of Physics, Chinese Academy of Science, Beijing 100080, People's Republic of China*

[3]*School of Physics and Astronomy, University of Glasgow, Glasgow G12 8QQ, United Kingdom*

[4]*National Synchrotron Light Source, Brookhaven National Laboratory, Upton, New York 11973, USA*

(Received 15 September 2009; revised manuscript received 8 October 2010; published 13 December 2010)

Temperature and bias voltage-dependent transport characteristics are presented for double magnetic tunnel junctions (DMTJs) with self-assembled NiFe nanoparticles embedded between insulating alumina barriers. The junctions with embedded nanoparticles are compared to junctions with a single barrier of comparable size and growth conditions. The embedded particles are characterized using x-ray absorption spectroscopy, transmission electron microscopy, and magnetometry techniques, showing that they are unoxidized and remain superparamagnetic to liquid helium temperatures. The tunneling magnetoresistance (TMR) for the DMTJs is lower than the control samples, however, for the DMTJs an enhancement in TMR is seen in the Coulomb blockade region. Fitting the transport data in this region supports the theory that cotunneling is the dominant electron transport process within the Coulomb blockade region, sequential tunneling being suppressed. We therefore see an enhanced TMR attributed to the change in the tunneling process due to the interplay of the Coulomb blockade and spin-dependent tunneling through superparamagnetic nanoparticles, and develop a simple model to quantify the effect, based on the fact that our nanoparticles will appear blocked when measured on femtosecond tunneling time scales.

DOI: 10.1103/PhysRevB.82.214415 PACS number(s): 75.70.−i, 73.23.Hk, 85.75.−d, 72.25.−b

I. INTRODUCTION

There are now a wide range of spintronic devices[1] that utilize the interplay of the spin degree of freedom with other physical effects. One such device is a type of double magnetic tunnel junction (DMTJ) where the central electrode is a nanoparticle that is small enough that charging effects become significant, resulting in single electron behavior.[2] In this case spin-dependent effects and Coulomb blockade physics combine[3] to produce fascinating results,[4] such as spin-accumulation,[5,6] tunneling anisotropic magnetoresistance,[7] Kondo physics,[8] enhanced tunnel magnetoresistance (TMR),[9,10] and electromotive force generation.[11]

TMR is the change in resistance through a magnetic tunnel junction device when the relative magnetization direction of two of the electrodes is switched. It is quantitatively defined as a fractional change in resistance $(R_{AP}-R_P)/R_P$, where R_P and R_{AP} are the resistances of the junction with the electrodes magnetic moments aligned parallel (P) and antiparallel (AP), respectively. The Coulomb blockade is the suppression of tunneling through a particle within an insulating barrier due to the increase in electrostatic charging energy when introducing additional electrons onto the particle. When this charging energy, $E_c=e^2/2C$ (where C is the capacitance of the particle) is larger than thermal fluctuations the conventional (sequential) electron tunneling is blocked, i.e., there is a Coulomb blockade when $E_c \gg k_B T$. However, when this condition holds, conduction is still possible via a virtual charging of the central electrode where two tunneling events take place simultaneously, known as cotunneling. TMR enhancement is theoretically predicted when cotunneling is the dominant electron transport process.[9,12]

Previous devices of this kind[5,8,9,13–15] have incorporated the nanoparticle moment alignment in the parallel or antiparallel state with respect to the outer electrodes. Here however, we investigate the effect on the spin transport when the two states are defined by the outer electrodes and the nanoparticle moments are randomly oriented. We use the common spintronic material Permalloy (NiFe), the low magnetocrystalline anisotropy of NiFe ensures that our nanoparticles are superparamagnetic at all experimentally accessible temperatures, meaning that the electrons must tunnel through an array of islands in which the spin quantization axis is randomly fluctuating due to thermal excitations. We previously published our preliminary findings, restricted to low temperature, on these samples in Ref. 16. Here we present a full temperature-dependent study of the magnetotransport in these junctions.

It is often assumed in DMTJ studies that metallic nanoparticles embedded within in an oxide simply stay in a metallic state with insignificant reaction with their surroundings. It is known however that a metal in contact with an oxide is liable to oxidize to some degree[17,18] and also that nanoparticles have been shown to have higher than expected reactivity.[19] Therefore, we also report here additional characterization of our nanoparticles using x-ray absorption spectroscopy (XAS) and transmission electron microscopy (TEM).

An enhancement of the TMR value of $2(1-P^2)$ (where is P is the electrode polarization)[9,12] is predicted when in the cotunneling regime and the two junctions of the DMTJ are in the same state, i.e., both parallel or antiparallel, the enhance-

ment for a system such as ours where both junctions are not necessarily in the same state is not clear. Here, we report in full our observation of the crossover from sequential tunneling dominating at higher temperatures and bias voltages to cotunneling dominating in the Coulomb blockade region but above the superparamagnetic blocking temperature of the nanoparticles, and also develop a simple model to treat this sample configuration to show that the cotunneling enhancement of TMR is maintained even when tunneling through superparamagnetic nanoparticles with fluctuating moment directions where the TMR is defined by the outer electrodes.

II. METHODS

DMTJs with nanoparticles embedded in the insulating barrier were deposited with the following layer configuration:

$$[\text{wafer(Si/SiO}_2)]\text{Ru(20)/Ni}_{79}\text{Fe}_{21}(3)/\text{Ir}_{22}\text{Mn}_{78}(15)/\text{Co}_{90}\text{Fe}_{10}(4)/\text{Ru}(0.9)/\text{Co}_{40}\text{Fe}_{40}\text{B}_{20}(4)/\text{AlO}_x(1)/\text{Ni}_{79}\text{Fe}_{21}(0.3)/\text{AlO}_x(1)/\text{Co}_{40}\text{Fe}_{40}\text{B}_{20}(4)/\text{Ru}(5)$$

(units nm). The central NiFe layer is denoted as a nominal average thickness, since we would expect the layer to form nanoparticles, aggregating into islands due to surface energy differences.[20] Control samples without nanoparticles were also produced in the same sputtering run: the same stack was grown in the same conditions as the DMTJs with the exception of the middle NiFe layer but including the separate growth of the two AlO_x barrier layers. The samples were deposited by magnetron sputtering in a 0.6 mTorr Ar atmosphere with a 100 Oe field applied to define the pinning direction. The oxide was created by depositing a 1 nm Al film in the conditions described above, followed by a plasma oxidation process used to create the oxide barrier in a 17:50 $Ar:O_2$ atmosphere.[21]

Samples with the arrangement $[\text{wafer(Si/SiO}_2)]/\text{Ru(10)/AlO}_x(1)/\text{Ni}_{79}\text{Fe}_{21}(0.3)/\text{AlO}_x(1)$ were also produced as sheet films to make it possible to characterize the properties of the NiFe nanoparticles independently of the magnetic stack. These were deposited in the same sputtering run as the full junctions. XAS measurements were made on the above sample and also the same stack but without the top AlO_x layer, along with similar samples with 0.8 nm of NiFe for comparison of oxidation state. All samples were measured in the as-deposited state. The XAS measurements were carried out at the U4B beamline at the National Synchrotron Light Source (NSLS), Brookhaven National Laboratory.[22] There, the soft x-ray beam used was linearly polarized with an energy resolution <0.7 eV at the Co L_3 edge. The data were collected in the total electron yield mode, with the sample current normalized to an Au grid beam monitor mounted upstream of the sample chamber. Magnetic characterization of the nanoparticles was performed using a variable temperature vibrating sample magnetometer (VSM).[16]

The junction shapes were defined using photolithography and ion milling to produce junctions with active areas of $7 \times 14\ \mu m^2$. The electrical measurements to be discussed were taken at a range of temperatures with the standard four-probe arrangement in a liquid He cryostat. The control samples yielded low-temperature ($T=3$ K) TMR in excess of 70% showing these conditions to be appropriate for creating high-quality AlO_x tunnel barriers.

Cross-section TEM specimens of the junctions measured in this study were prepared by a focused ion beam (FIB) mill and lift-out technique using an FEI Nova 200 FIB system and an Omniprobe 100 micromanipulator. A 30 keV Ga^+ ion beam was used to cut a section through the bulk of the MTJs used for the transport measurements. Prior to ion milling, the samples were coated with a Pt layer to protect the sample surface from ion beam damage. Bright field images of the cross sections were acquired using an FEI Tecnai T20 TEM.

III. RESULTS

A. Nanoparticle characterization: XAS

The Coulomb blockade requires a conducting, i.e., metallic, nanoparticle island. However, transition metals such as Fe or Ni are chemically reactive and easily oxidized. A useful technique to determine the oxidation state of the embedded particles is XAS, as clear differences can be seen in the absorption spectra for the metallic or oxidized states due to a change in the binding energies of the core electrons. The samples used here have NiFe particles embedded in the oxide or on the surface of the oxide exposed to atmosphere, the latter used as the comparison to what should be the fully oxidized state.

While both the Fe and Ni edges showed evidence of oxidation, we focus on the Fe edges as the differences are more distinct (for all samples evidence of oxidation at the Ni edges is small, a consequence of the lower reactivity of Ni, but following the same trend as the Fe edges). Figure 1 shows XAS spectra of the Fe edges, the curves have been normalized to the L_3 peak height and a linear background subtracted, then offset for clarity. There is some oxidation present in all of the samples, evident as the shoulder to the right of the L_3 edge ($\sim$707 eV) and the multiple peaks at the L_2 edge ($\sim$720 eV). For comparison with an oxidized nanoparticle sample, also shown in Fig. 1, are larger particles (0.8 nm NiFe layer) showing a considerable amount of oxidation when embedded in the barrier, which increases still further

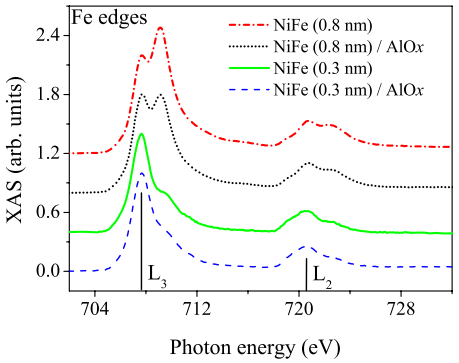

FIG. 1. (Color online) XAS data collected at room temperature in the vicinity of the Fe L_3 and L_2 edges (tabulated values marked with ticks). Samples measured: $[\text{wafer}(\text{Si}/\text{SiO}_2)]/\text{Ru}(10)/\text{AlO}_x(1)/x$, where x is shown as the legend. The NiFe thickness given is for nominal film growth thickness rather than particle size. The curves have been normalized and offset for clarity.

when they lie on the sample surface. The Fe peak is still visible however, suggesting we have a metallic core surrounded by an oxide shell of varying thickness. For the smaller embedded nanoparticles the Fe peak is strong and shows a comparably small amount of oxidation.

For the electron transport measurements it will be detrimental to the conservation of the spin through the system to have an oxide shell around the metallic nanoparticle, such as the case for the larger nanoparticles, since such oxides are generally ferrimagnetic or antiferromagnetic and will contain spin disorder at the interfaces. NiO and FeO are antiferromagnetic whereas α-Fe_2O_3 and Fe_3O_4 are ferrimagnetic.[23] From the splitting of the peaks in the Fe spectra it is most likely the Fe oxide is either α-Fe_2O_3 or Fe_3O_4. The first will not be conducive to spin conservation in the system and for the second, Fe_3O_4 has been shown to have be a highly spin-polarized half metal, however the resistance vs temperature data for the samples suggests that if present, the Fe_3O_4 does not play a dominant role in the conduction, as there is no evidence of a Verwey transition (which occurs in bulk at 119 K).[24] There are also possibly some Ni ferrites that complicate the picture further, however, it is clear that the smaller nanoparticles embedded in the barrier show the least oxidation with a large amount of metallic Fe (and, presumably, Ni), whatever the underlying oxidation mechanisms may be. Indeed, full junctions with the 0.8-nm-thick NiFe particle layer showed no TMR and will not be discussed further.

B. Nanoparticle characterization: Magnetization

VSM data for our samples were previously reported in Ref. 16, here we revisit the salient points. Magnetic nanoparticles, such as those embedded in these junctions will be superparamagnetic above their blocking temperature, defined as $T_B = KV/nk_B$,[25,26] where K is the anisotropy constant, V is the particle volume, and n is a constant depending on the experimental measurement time τ_m, $n \approx 25$ for $\tau_m \approx 1$ s.

The fit of the Langevin function to VSM data for the nanoparticles from the NiFe 0.3 nm film allowed us to extract a particle diameter of ~ 1.8 nm, assuming negligible oxidation.[16] This is an average diameter, as this method of fabricating nanoparticles will give some spread in particle size.[9] The VSM measurements confirmed that we have the situation $T > T_B$ for all measurement temperatures, i.e., our samples have sufficiently small KV product to remain superparamagnetic to very low temperatures. For instance, using this estimated diameter and assuming a typical value for NiFe of $K \approx 1$ kJ m^{-3},[27] we obtain a value for $T_B = KV/nk_B \approx 10$ mK. Shape anisotropy effects will be only an order of magnitude larger (assuming a demagnetizing factor $\mathcal{D} \approx 0.1$). It is instructive to compare our previous data,[16] where no hysteresis and a clear superparamagnetic Langevin behavior was observed at 5 K, with the obviously hysteretic magnetization loops for the slightly larger NiFe nanoparticles studied by Bručas *et al.*,[28] where the particles are blocked at the same temperature. We observed no such hysteresis.

These data indicate that the electrons tunneling through the DMTJs must pass through NiFe islands with thermally fluctuating moments. However, these will appear frozen on tunneling time scales, which are typically of order femtoseconds,[2] since typical superparamagnetic attempt frequencies are only $f_0 \sim 1-10$ GHz.[25] To the tunneling electrons the nanoparticles will appear as a stationary, randomly oriented, array of moments: a commonly employed analog of this is the Born-Oppenheimer approximation, where a vibrating lattice appears static, but disordered, to electrons, due to a similar comparison between electron scattering lifetimes and typical phonon frequencies.[29] Alternatively, from the point of view of superparamagnetism, we say that the value of $f_0 \tau_m \sim 10^{-5}$, so that our particles are indeed blocked for τ_m of the order of tunneling time scales.

C. Full junctions: TEM

A method commonly used to study magnetic nanoparticles is TEM, as was done in Refs. 8, 9, and 15, for instance. Figure 2 shows typical bright field TEM images of the DMTJ cross section. The cross section was prepared by FIB from the junction on which the transport data shown below were measured, once those experiments had been completed. The contrast levels within the images may been adjusted in order to highlight the structure within the barrier layers. The observed layer thicknesses are consistent with their nominal values. Figure 2 shows a cross-sectional image of the junction with a nominal thickness of 0.3 nm NiFe grown in the barrier. It is clear the NiFe layer has formed nanoparticles as expected, the particles appear spherical and with diameters in the range 1–2 nm, this agrees well with the fit to the VSM data. Any oxide shell is negligible in that it is not visible in the TEM, which is consistent with the XAS data.

D. Full junctions: Magnetotransport

We performed electrical measurements on both types of junctions: the control sample single magnetic tunnel junctions (SMTJs) and the DMTJs. Both showed nonlinear current-voltage (I-V) characteristics consistent with tunneling transport. In Fig. 3(a) we show TMR curves at 3 K for the control sample (for brevity labeled as SMTJ) and the

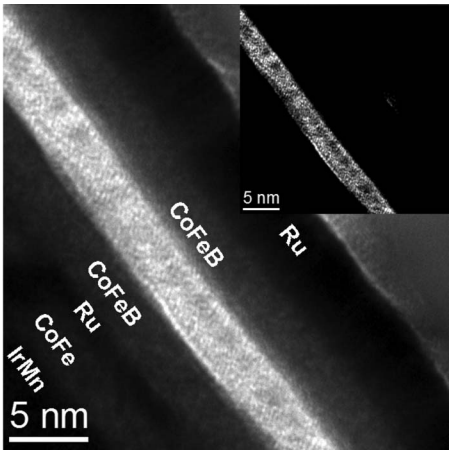

FIG. 2. Cross-sectional TEM images of the full junction stack with the 0.3 nm NiFe layer grown in between the AlO_x layers. The metallic layers are labeled, and the double barrier with nanoparticles appears as the white stripe in the middle of the image. The inset shows the same image with the contrast adjusted to make the presence of the nanoparticles in the barrier layer more clear.

DMTJ samples. The data were taken by measuring the current while applying a 10 mV bias and sweeping the magnetic field. The similarity in the shape of the curves confirms that for both types of junction the TMR arises from the relative magnetic alignment of the outer electrodes rather than the nanoparticle moment alignment. While the DMTJ has a lower TMR by roughly a factor of 2, the TMR ratio is still substantial, indicating that spin-polarized electrons can

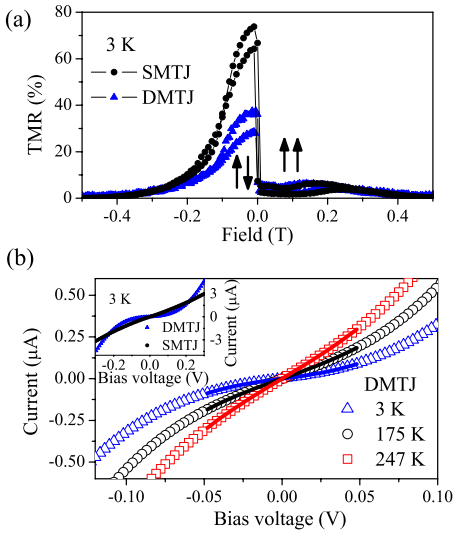

FIG. 3. (Color online) (a) Typical TMR curves at 3 K for SMTJ and DMTJ, taken with 10 mV applied bias. The arrows define the relative alignment the outer electrodes. (b) Current-voltage (*I-V*) characteristics for the junctions with NiFe (0.3 nm layer) embedded. The open symbols represent the data; the solid lines represent the fits to the data using Eq. (2). Inset: comparison between the SMTJ and DMTJ at 3 K. All curves in (b) were measured at $H=+150$ Oe, which corresponds to the outer electrodes being magnetized parallel, as shown in (a). The data measured at 3 K shown in panels (a) and (b) are replotted from Ref. 16.

traverse the superparamagnetic NiFe nanoclusters without complete loss of spin information. The drop from the SMTJ values could be due to the randomly oriented array of particle moments or from the lower spin polarization of the NiFe.[28]

Figure 3(b) shows *I-V* characteristics for the DMTJs, for measurements that were taken with a +150 Oe field, which aligns the electrode magnetization parallel, as we can see from Fig. 3(a). The inset shows typical curves at 3 K for the SMTJ and the DMTJ. The curves for the SMTJ show a typical tunneling shape, appearing nearly linear on this voltage bias scale.[30] The curves for the DMTJs have a markedly stronger bias dependence than the SMTJ and clear suppression of conductance at low bias which becomes more evident as the temperature decreases. This suppression of conduction is consistent with the sequential tunneling being blocked by the Coulomb blockade effect. The conductance never goes to zero if cotunneling is allowed, albeit cotunneling has a much lower tunneling rate than sequential tunneling. It should be noted that to exclude other conflicting transport or charging processes the barriers have been made to be as symmetric as possible and of high enough resistance (R_T) that the wave functions of the electrons are confined to the electrodes between tunneling events, i.e., the tunnel resistance $R_T > R_Q = h/2e^2$, the quantum of resistance. There is a balance to be made however, as cotunneling will be exponentially suppressed for $R_T/R_Q \to \infty$.[12]

In Fig. 4(a) we show differential resistance ($R=dV/dI$) curves numerically calculated from the *I-V* measurements with a −150 Oe field applied (the AP state of the outer electrodes) at a range of temperatures. Figure 4(b) shows similar data for a +150 Oe field applied (the P state). The insets show the dV/dI data for the control SMTJ sample at two temperatures in order that the shape of the curves may be compared. All these data have been smoothed over a 3 mV window. The resistance of both types of junctions rises as the samples are cooled, which is confirmation of having tunneling as the primary method of conduction.[31]

The dV/dI curves in Figs. 4(a) and 4(b) show strong peaks around zero bias which become more prominent as the temperature decreases. The peaks are far more pronounced than the bias dependence observed in the SMTJs, which is fairly typical of that for magnetic tunnel junctions.[32] The insets both show asymmetry in the curves, the high TMR (for AlO_x junctions) suggests this can be attributed to the band structure of the electrodes caused by minor deviations from optimal oxidation of the bottom electrode, as the electrodes are both formed form the same composition of CoFeB.[33,34] The DMTJ dV/dI curves are symmetric; here the dominant effect in limiting the number of conduction channels across the junction will be the blocking of sequential tunneling, we would expect this process to be symmetric in bias ($|V| \lesssim E_c$). Moreover, for the DMTJs it is clear that the low-bias temperature dependence of R is very much stronger than for the SMTJ, which is another signature that cotunneling is the dominant process for low V, low T transport in the DMTJ.[12]

Figure 4(c) shows the TMR of the DMTJ vs bias voltage and temperature dependence, derived from the full set of *I-V* curves. The TMR map clearly shows steep increases in the

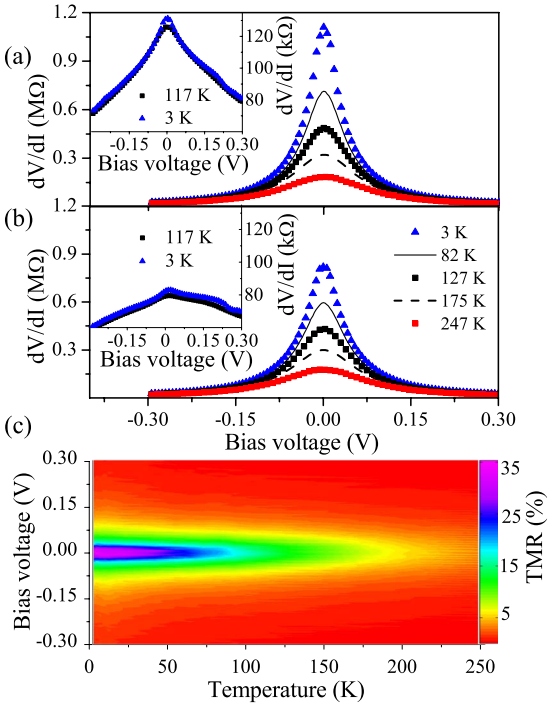

FIG. 4. (Color online) (a) Typical differential resistance vs bias voltage (R vs V) data for the DMTJs in the antiparallel outer electrode arrangement, at various temperatures. Inset: R vs V for the SMTJ at two temperatures. (b) Typical R vs V data for the DMTJs in the parallel outer electrode arrangement, various temperatures. Inset: R vs V for the SMTJ at two temperatures. (c) TMR vs bias voltage and temperature, derived from the full set of I-V curves. The data measured at 3 K shown in panels (b) and (c) are replotted from Ref. 16.

TMR at low temperature ($T \lesssim 100$ K) and bias ($V \lesssim 75$ mV). Rather than a distinct change as the system enters the Coulomb blockade region, the increase in TMR is smooth due to a crossover where sequential and cotunneling play comparable roles in the conduction.[12] In this system the particle sizes have a small spread which will give a range of charging energies, for this size of junction there will be a number of parallel conduction paths which unblock at different energies. From the TEM we can see a spread of between $\sim 1-2$ nm; taking the capacitance to be $C=2\pi\varepsilon_0\varepsilon_r d$, where $\varepsilon_r=8$ and d is the diameter of the nanoparticles, we can calculate the corresponding range of Coulomb blockade voltages,[35] $V_C=e/2C$, to give the range 90–180 mV, which correlates well with the onset of the Coulomb blockade characteristics in our transport data.

IV. DISCUSSION

Theory gives the following expression for the sub-Coulomb gap I-V characteristic for inelastic cotunneling:[36]

$$I(V) = \left(\frac{\hbar}{3\pi e^2 R_T^2 E_c^2}\right)[(2\pi k_B T)^2 V + e^2 V^3], \quad (1)$$

where R_T is the tunnel resistance and E_c is the charging energy.[37] There are contributions to conductance that are linear and cubic in V. In this instance, taking a phenomenological view, we fitted our data with the expression

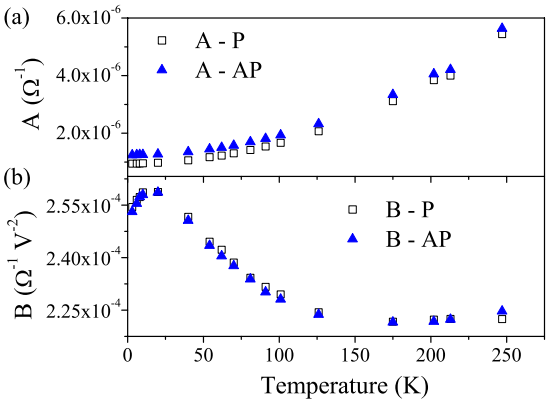

FIG. 5. (Color online) (a) Variation in the linear (A) and (b) cubic (B) conductance coefficients with temperature T from fits to the DMTJ I-V data. P and AP denote parallel and antiparallel alignments of the outer electrodes, respectively.

$$I(V) = AV + BV^3 \quad (2)$$

between ± 50 mV, i.e., only well within the region where we have enhanced TMR and expect cotunneling to dominate and where the usual tunneling contributions are almost Ohmic. Examples of the fits are shown in Fig. 3(b) as solid lines. Figure 5 shows the coefficients yielded by fitting the I-V curves of the DMTJ at a range of temperatures. (The 3 K values for A and B differ slightly from those we reported in Ref. 16, as there we fitted the data across the full range of voltage biases applied, rather than restricting ourselves to the cotunneling regime.) The coefficient A (the linear term representing the Ohmic part of the conductance) shows a strong increase with as the temperature, rising by roughly a factor of 5, a much larger fractional change than B (cubic term). This implies that the mechanism of electron transport is dominated by cotunneling at low temperatures due to the suppression of sequential tunneling currents rather than a large increase in cotunneling rate.

In practice there are potentially additional contributions to the conductance that are linear in V at low bias, such as sequential tunneling through larger islands where $k_B T > E_c$, as well as any leakage current through the system. Comparing Eq. (1) with Eq. (2), the ratio of the coefficients B/A should yield an ideal value of $(e/2\pi k_B T)^2$ in which the only experimental variable is the temperature. At a temperature of 3 K this gives an ideal ratio of $\sim 4\times 10^5$ while the experimental value of B/A for the DMTJ is only $\sim 3\times 10^2$. This discrepancy in the DMTJ value compared with the theoretical value can be attributed to additional conductance contributions which are linear in V (at low bias), such as discussed above. It is important to note however that for the SMTJ at 3 K $B/A \sim 1$, two orders of magnitude smaller still, the I-V characteristics are much more linear due to the absence of Coulomb blockade effects.

Now that we have established that inelastic cotunneling is the dominant mechanism for transport for $eV, k_B T \ll E_c$, we examine our data in terms of the predictions for enhanced

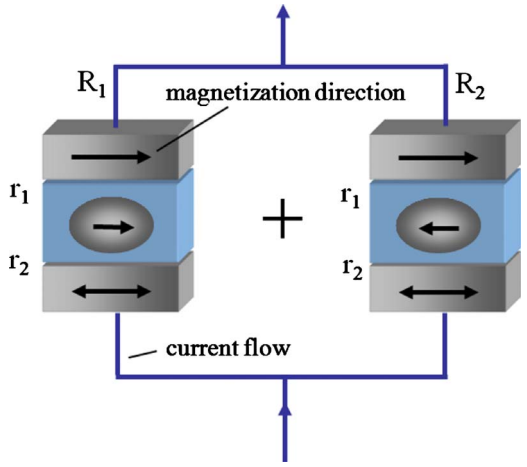

FIG. 6. (Color online) Schematic of two-state model of tunnel current flow through the DMTJ; the bottom outer electrodes (the DMTJ free layer) will either both be parallel or both antiparallel with respect to the top outer electrodes (the DMTJ pinned layer).

TMR in this regime.[12] TMR has been theoretically predicted to be enhanced when cotunneling is the dominant conduction process, owing to the total junction resistance being proportional to the sum of the single junction resistances (r_1 and r_2 in Fig. 6) for the sequential tunneling regime and proportional to the product for the cotunneling regime, reflecting its coherent nature.[12] The previously predicted enhancement simplifies to $2(1-P^2)$, where P is the effective polarization of the electrodes. This simplification, however, is for junctions where r_1 and r_2 are in the parallel or antiparallel state simultaneously. Therefore the previous enhancement is not valid in this study where the parallel/antiparallel states come from the alignment of the outer electrodes and the nanoparticles are superparamagnetic; as it is not necessarily the case that r_1 and r_2 will both be in the parallel (or antiparallel) state simultaneously, a different treatment is required.

As a simple model that captures the essential physics of this situation we sum the resistances of two parallel conduction channels (R_1 and R_2 in Fig. 6) with the nanoparticle alignment as one direction or the other collinear to the electrode magnetization, repeating this for when the outer electrodes are aligned either parallel or antiparallel. Summing our parallel conducting channels we obtain equations for total junction resistance in the four situations, the parallel and antiparallel electrode arrangements in the sequential and cotunneling regimes (details are shown in the Appendix). The TMR ratio may then be calculated in each regime as $(R_{AP}/R_P)-1$.

These calculations can then be used with the results of the DMTJ measurements to quantify the expected TMR for the low-temperature TMR without the Coulomb blockade, and hence calculate the enhancement caused by cotunneling transport. At $T=3$ K, the measured low-bias value for the TMR is $\sim 35\%$, with $R_{AP}=1.11\times10^6$ Ω and $R_P=0.82\times10^6$ Ω, corresponding to the cotunneling regime. Inverting Eqs. (A3) and (A4), we obtain a pair of simultaneous equations that may be solved to give $r_{\uparrow\uparrow}$ and $r_{\uparrow\downarrow}$, which we then inserted into Eqs. (A1) and (A2) to predict TMR in the sequential regime to be $\sim 18\%$. This is close to the value that may obtained by extrapolating the high-bias (sequential regime) trend in the DMTJ TMR(V) at this temperature back to $V=0$. It is also roughly in accord with a similar extrapolation of the high temperature trend back to He temperatures. Therefore, we see a roughly twofold enhancement in the TMR for the DMTJs due to cotunneling, in spite of tunneling through superparamagnetic nanoparticles with fluctuating moments.

V. SUMMARY

We have fabricated and studied AlO_x-based double magnetic tunnel junctions with NiFe nanoparticles embedded within the oxide barrier, these have been compared with control samples without nanoparticles. The nanoparticles were grown by self-assembly from a NiFe thin film deposited on the oxide layer. The electrical results for the DMTJs were compared to control SMTJs.

The two types of junctions showed distinctly different I-V characteristics: the DMTJs showed a highly nonlinear I-V characteristic, which leads to pronounced low-bias peaks in the differential resistance and TMR ratio that are absent from the data for the SMTJ. The results of fitting to the I-V data, as well as the enhancement in TMR are both consistent with cotunneling being the dominant electron transport process at low temperature and bias, where sequential tunneling is suppressed by the Coulomb blockade.[12] The significant TMR of the DMTJ in both the sequential and cotunneling regimes indicate that spin information is preserved during the cotunneling process, in spite of the fact that the nanoparticles are superparamagnetic and hence have fluctuating moments. We treat this in terms of a simple model where the superparamagnetic moments are treated as frozen on tunneling time scales, allowing us to estimate cotunneling enhancement of the TMR in this previously unexplored device geometry. Previous observations of the enhancement effect included the magnetic moment of nanoparticles in the P and AP states,[8,9,13] the switching fields of which can be difficult to control. In our geometry the TMR enhancement is available at the switching field of a conventional MTJ free layer, which may easily be engineered. Potentially combining this device geometry with room-temperature Coulomb blockade effects[38] will allow the cotunneling enhancement to be exploited in practical devices.[10]

ACKNOWLEDGMENTS

We would like to acknowledge support from the U.K. EPSRC (Engineering and Physical Sciences Research Council), the Royal Society, and the National Natural Science Foundation of China, as well as the U.S. Department of Energy, Office of Basic Energy Sciences for provision of NSLS beamtime.

APPENDIX: RESISTANCE FORMULAS

Here we set out some details of the formulas used in our model, described in Sec. IV. We define r_1 as the tunnel resistance between electrode 1 and a nanocluster, similarly

r_2 is the tunnel resistance between electrode 2 and the nanocluster. For the calculation of the total junction resistance (and consequently the TMR) the single junction resistances r_1 and r_2 (see Fig. 6) are either summed or multiplied for sequential or cotunneling respectively, following previous theoretical work,[12] to give the total resistance through an island. Since in our structures the electrodes and barriers are nominally identical we assume that $r_1=r_2$. Both r_1 and r_2 then have two possible values $r^{\uparrow\uparrow}$ and $r^{\uparrow\downarrow}$, which are the resistances of either single junction when the moments in the electrode and island are parallel or antiparallel, respectively.

As discussed in Sec. III B, we treat the magnetization states of the islands as a static, frozen array of random moments, in analogy to the Born-Oppenheimer approximation. To have a simple, analytical model that is physically transparent, we assume here that exactly half of the island moments point to the left and the other half to the right. In terms of the TMR ratio only the proportion of islands pointing in the each direction is relevant. We therefore treat two double junctions in parallel, one with the island in each state, as shown in Fig. 6, the overall resistances of which are R_1 and R_2. The total resistance is then simply $R_1R_2/(R_1+R_2)$.

The outer electrodes can take up either a parallel or antiparallel state. The equations for the total resistance in each state are as follows. For the sequential tunneling regime, the resistance with the electrodes in the parallel state is given by

$$R_{\mathrm{P}}^{\mathrm{seq}} = \frac{4r^{\uparrow\uparrow}r^{\uparrow\downarrow}}{2r^{\uparrow\uparrow}+2r^{\uparrow\downarrow}} \tag{A1}$$

while the antiparallel resistance is given by

$$R_{\mathrm{AP}}^{\mathrm{seq}} = \frac{(r^{\uparrow\uparrow})^2+(r^{\uparrow\downarrow})^2+2r^{\uparrow\uparrow}r^{\uparrow\downarrow}}{2r^{\uparrow\uparrow}+2r^{\uparrow\downarrow}}. \tag{A2}$$

In the cotunneling regime, the parallel resistance is

$$R_{\mathrm{P}}^{\mathrm{co}} = \frac{(r^{\uparrow\uparrow})^2(r^{\uparrow\downarrow})^2}{(r^{\uparrow\uparrow})^2+(r^{\uparrow\downarrow})^2} \tag{A3}$$

and the antiparallel resistance is

$$R_{\mathrm{AP}}^{\mathrm{co}} = \frac{r^{\uparrow\uparrow}r^{\uparrow\downarrow}}{2}. \tag{A4}$$

*phy9kjd@leeds.ac.uk; www.stoner.leeds.ac.uk
†c.h.marrows@leeds.ac.uk

[1] I. Žutić, J. Fabian, and S. D. Sarma, Rev. Mod. Phys. **76**, 323 (2004).
[2] K. K. Likharev, IBM J. Res. Dev. **32**, 144 (1988).
[3] J. Barnaś and A. Fert, Phys. Rev. Lett. **80**, 1058 (1998).
[4] P. Seneor, A. Bernand-Mantel, and F. Petroff, J. Phys.: Condens. Matter **19**, 165222 (2007).
[5] A. Bernand-Mantel, P. Seneor, N. Lidgi, M. Muñoz, V. Cros, S. Fusil, K. Bouzehouane, C. Deranlot, A. Vaures, F. Petroff, and A. Fert, Appl. Phys. Lett. **89**, 062502 (2006).
[6] K. Yakushiji, F. Ernult, H. Imamura, K. Yamane, S. Mitani, K. Takanashi, S. Takahashi, S. Maekawa, and H. Fujimori, Nature Mater. **4**, 57 (2005).
[7] A. Bernand-Mantel, P. Seneor, K. Bouzehouane, S. Fusil, C. Deranlot, F. Petroff, and A. Fert, Nat. Phys. **5**, 920 (2009).
[8] H. Yang, S.-H. Yang, and S. S. P. Parkin, Nano Lett. **8**, 340 (2008).
[9] H. Sukegawa, S. Nakamura, A. Hirohata, N. Tezuka, and K. Inomata, Phys. Rev. Lett. **94**, 068304 (2005).
[10] L. Jiang, H. Naganuma, M. Oogane, and Y. Ando, Appl. Phys. Express **2**, 083002 (2009).
[11] P. N. Hai, S. Ohya, M. Tanaka, S. E. Barnes, and S. Maekawa, Nature (London) **458**, 489 (2009).
[12] S. Takahashi and S. Maekawa, Phys. Rev. Lett. **80**, 1758 (1998).
[13] L. F. Schelp, A. Fert, F. Fettar, P. Holody, S. F. Lee, J. L. Maurice, F. Petroff, and A. Vaurès, Phys. Rev. B **56**, R5747 (1997).
[14] F. Fettar, S.-F. Lee, F. Petroff, A. Vaurès, P. Holody, L. F. Schelp, and A. Fert, Phys. Rev. B **65**, 174415 (2002).
[15] F. Ernult, K. Yamane, S. Mitani, K. Yakushiji, K. Takanashi, Y. K. Takahashi, and K. Hono, Appl. Phys. Lett. **84**, 3106 (2004).
[16] K. J. Dempsey, A. T. Hindmarch, C. H. Marrows, H.-X. Wei, Q.-H. Qin, Z.-C. Wen, and X.-F. Han, J. Appl. Phys. **105**, 07C923 (2009).
[17] T. J. Regan, H. Ohldag, C. Stamm, F. Nolting, J. Lüning, J. Stöhr, and R. L. White, Phys. Rev. B **64**, 214422 (2001).
[18] A. T. Hindmarch, K. J. Dempsey, D. Ciudad, E. Negusse, D. A. Arena, and C. H. Marrows, Appl. Phys. Lett. **96**, 092501 (2010).
[19] B. Hvolbæk, T. V. W. Janssens, B. S. Clausen, H. Falsig, C. H. Christensen, and J. K. Nørskov, Nanotoday **2**, 14 (2007).
[20] C. T. Campbell, Surf. Sci. Rep. **27**, 1 (1997).
[21] H. X. Wei, Q. H. Qin, M. Ma, R. Sharif, and X. F. Han, J. Appl. Phys. **101**, 09B501 (2007).
[22] http://www.nsls.bnl.gov/beamlines/beamline.asp?blid=u4b
[23] T. Koide, T. Shidara, H. Fukutani, K. Yamaguchi, A. Fujimori, and S. Kimura, Phys. Rev. B **44**, 4697 (1991).
[24] W. Wang, M. Yu, M. Batzill, J. He, U. Diebold, and J. Tang, Phys. Rev. B **73**, 134412 (2006).
[25] A. Aharoni, *Introduction to the Theory of Ferromagnetism* (Oxford University Press, Oxford, 1996).
[26] S. Bedanta and W. Kleemann, J. Phys. D: Appl. Phys. **42**, 013001 (2009).
[27] J. M. D. Coey, *Magnetism and Magnetic Materials* (Cambridge University Press, New York, 2010).
[28] R. Bručas, M. Hanson, P. Apell, P. Nordblad, R. Gunnarsson, and B. Hjörvarsson, Phys. Rev. B **81**, 224437 (2010).
[29] J. M. Ziman, *Electrons and Phonons*, Oxford Classic Texts in the Physical Sciences (Oxford University Press, Oxford, 2001).
[30] J. G. Simmons, J. Appl. Phys. **34**, 1793 (1963).
[31] B. J. Jönsson-Åkerman, R. Escudero, C. Leighton, S. Kim, I. K. Schuller, and D. A. Rabson, Appl. Phys. Lett. **77**, 1870 (2000).
[32] S. Zhang, P. M. Levy, A. C. Marley, and S. S. P. Parkin, Phys. Rev. Lett. **79**, 3744 (1997).
[33] A. T. Hindmarch, C. H. Marrows, and B. J. Hickey, Phys. Rev. B **72**, 060406(R) (2005).
[34] A. H. Davis and J. M. MacLaren, J. Appl. Phys. **91**, 7023 (2002).

[35] E. Schabowska and J. Szczeklik, Thin Solid Films **75**, 177 (1981).
[36] The rate of elastic cotunneling is small and only significant at very low temperatures, see Ref. 37.
[37] D. V. Averin and Y. V. Nazarov, *Single Charge Tunneling: Coulomb Blockade Phenomena in Nanostructures* (Plenum Press, New York, 1992), pp. 217–247.
[38] V. Ray, R. Subramaniana, P. Bhadrachalam, L.-C. Ma, C.-U. Kim, and S. J. Koh, Nat. Nanotechnol. **3**, 603 (2008).